JEE Journal of Ecological Engineering

Journal of Ecological Engineering, 2026, 27(5), 444–459
https://doi.org/10.12911/22998993/216147
ISSN 2299–8993, License CC-BY 4.0

Received: 2025.12.18
Accepted: 2026.03.16
Published: 2026.04.01

Bio-based chitosan with calcium ions and chitosan-tannic acid coagulation systems for efficient microplastic removal: Mechanistic insights and artificial neural network predictive modeling

Buty Kurnia Hamzani[1], Deswati Deswati[1*], Mai Efdi[1], Yefrida Yefrida[1], Adewirli Putra[2]

[1] Department of Chemistry, Faculty of Mathematics and Natural Science, Universitas Andalas, Padang, 25163, Indonesia
[2] Department of Medical Laboratory Technology, Syedza Saintika University, Padang, 25132, Indonesia
* Corresponding author's e-mail: deswati@sci.unand.ac.id

ABSTRACT

Microplastic pollution from polyethylene (PE) and polystyrene (PS) remains difficult to remediate using conventional metal-based coagulants due to sludge generation and environmental risks. This study develops and evaluates a fully bio-based, Fe/Al-free coagulation system using chitosan enhanced with calcium ions (Ca^{2+}) and tannic acid. Coagulation experiments were performed under controlled variations of pH, chitosan dosage, slow mixing duration, and coagulant aids. Removal performance was quantified gravimetrically, while mechanisms were elucidated through zeta potential, ATR-FTIR, and SEM analyses. Chitosan showed markedly higher coagulation efficiency at near-neutral pH, achieving 18.53% removal for PE and 47.66% for PS. The incorporation of Ca^{2+} or tannic acid further improved removal to 27.13% and 65.03%, respectively. Mechanistic characterization demonstrated that charge neutralization, ionic bridging, hydrogen bonding, hydrophobic interactions, and π–π stacking collectively govern microplastic aggregation. Ca^{2+} promoted electrical double-layer compression and enhanced floc compactness, whereas tannic acid strengthened adsorption through phenolic-amine interactions and aromatic affinity with PS. An artificial neural network (ANN) model incorporating six operational parameters successfully captured the nonlinear relationships influencing removal efficiency, showing good predictive performance within the experimental domain and providing insights into parameter contributions. Overall, the findings highlight the potential of chitosan-based systems as sustainable, metal-free alternatives for microplastic mitigation. The synergistic role of Ca^{2+} and tannic acid offers a pathway toward scalable, environmentally safe coagulation technologies for water treatment applications.

Keywords: ANN, chitosan, coagulation, microplastics, polyethylene–polystyrene.

INTRODUCTION

Microplastic pollution has emerged as a critical global concern due to its persistence, bioaccumulation potential, and adverse impacts on aquatic ecosystems and human health (Du et al., 2021). Polyethylene (PE) and polystyrene (PS) are among the most widely detected microplastics in aquatic environments, originating from extensive industrial use and exhibiting strong chemical stability (Hidalgo-Ruz et al., 2012; Koelmans et al., 2019). Their contrasting physicochemical properties PE being highly hydrophobic and buoyant, while PS possesses aromatic π–π reactivity, create distinct challenges for their removal in water treatment systems (Arvaniti et al., 2021; Zhou et al., 2025). Conventional techniques such as filtration and sedimentation often show limited effectiveness for microplastics smaller than 500 µm (Avazpour and Noshadi, 2024).

Although coagulation–flocculation with $FeCl_3$, PAC, or alum is frequently applied and generally effective (Li et al., 2022; Ma et al., 2019; Zhang et al., 2022), these coagulants generate

chemically reactive sludge and may introduce metal residues into treated water, raising environmental and regulatory concerns (Izabela, 2020; Sotero-Santos et al., 2007). Consequently, natural coagulants such as chitosan have gained growing attention due to their biodegradability, non-toxicity, and strong electrostatic affinity for negatively charged particles (Sixto-Berrocal et al., 2023). Previous studies have demonstrated that combining chitosan with Fe- or Al-based coagulants can enhance microplastic removal efficiency (Eamrat et al., 2024; He et al., 2024; Huang et al., 2023; Raj et al., 2024).

However, despite these advancements, current applications of chitosan remain largely dependent on metal-based systems. Although Ca^{2+} and tannic acid have individually shown potential as environmentally benign enhancers in water treatment, a fully metal-free coagulation system integrating chitosan with Ca^{2+} and tannic acid for microplastic removal remains unexplored. This gap is critical given the global demand for sustainable treatment technologies that minimize chemical toxicity while maintaining high removal performance.

Recent developments (2023–2025) highlight increased interest in green coagulants, hybrid biopolymer systems, and data-driven modeling for process optimization (Avazpour and Noshadi, 2024; He et al., 2024) Nevertheless, no study to date has systematically investigated the synergistic interactions of chitosan-Ca^{2+} and chitosan-tannic acid complexes, nor analyzed their combined physicochemical mechanisms using zeta potential, ATR-FTIR, and SEM under standardized conditions. Furthermore, the integration of interpretable artificial neural network (ANN) modeling to predict microplastic removal in a fully metal-free biocoagulation system has not been reported.

To address this gap, the present study develops and evaluates a bio-based, Fe/Al-free coagulation system utilizing chitosan with Ca^{2+} and tannic acid as functional enhancers. Through controlled coagulation experiments, mechanistic characterization, and ANN predictive modeling, this work aims to elucidate the synergistic interactions governing microplastic removal and provide a foundation for scalable, environmentally safe water treatment technologies

MATERIALS AND METHODS

Experimental materials

The chemical reagents used were chitosan (Sigma-Aldrich), tannic acid and calcium chloride ($CaCl_2$) were both obtained from Merck, sodium hydroxide (NaOH, Merck), hydrochloric acid (HCl, Merck), 95% Ethanol (Onemed), and deionized water. Fresh stock solutions of chitosan, tannic acid, and calcium chloride ($CaCl_2$) were prepared immediately before each experiment to maintain solution stability. Additional materials included filter paper, aluminum foil, PE and PS microplastics, which were sourced from a commercial online supplier based in Indonesia.

Microplastic preparation

PE microplastics (<500 μm) were obtained by sieving through a 500 μm mesh, while PS microplastics were ground and sieved to achieve a comparable size. Both were cleaned with 1 M HCl, rinsed with deionized water, and dried at 40–50 °C before storage in sealed containers. The brief HCl rinsing was applied solely as a cleaning step to remove surface impurities. Surface characteristics were analyzed using ATR-FTIR, zeta potential analysis, and SEM prior to coagulation experiments. ATR-FTIR was used to identify surface functional groups, SEM to examine particle morphology, and zeta potential analysis to determine the initial surface charge and colloidal stability of the microplastics, which are critical factors governing their coagulation behavior.

Coagulation procedure

Coagulation experiments were conducted in 250 mL glass beakers using a Heidolph magnetic stirrer to assess the removal efficiency of PE and PS microplastics, with 100 mg of microplastics per run (Huang et al., 2023). The process optimization involved three stages: (i) pH variation (5–9) at 100 mg/L chitosan, (ii) chitosan dosage optimization (0–300 mg/L), and (iii) slow mixing time optimization (0–25 min). Rapid mixing was performed at 400 rpm for 30 s, followed by slow mixing, while pH adjustments were made using 0.1 M HCl or NaOH. Combination treatments incorporated calcium chloride ($CaCl_2$) and tannic acid (0–500 mg/L) as coagulant aids. After

coagulation, suspensions were allowed to settle for 30–60 min prior to analysis.

Separation and quantification

After coagulation, uncoagulated microplastics in the upper were carefully collected, washed with 1 M HCl, filtered, and oven-dried at 60 °C to a constant weight (Chen et al., 2024). The residual microplastic mass was quantified gravimetrically, a reliable method previously validated for coagulation studies (Huang et al., 2023; Ma et al., 2019; Monira et al., 2021; Zhou et al., 2021). Removal efficiency was calculated from the mass difference before (W_0) and after (W_t) coagulation using (Avazpour and Noshadi, 2024):

$$Removal\ Efficiency\ (\%) = \frac{W_0 - Wt}{W_0} \times 100\% \quad (1)$$

where: *Wo* – microplastic initial weight, *Wt* – remaining microplastic weight, blank correction was applied only to *PS* microplastics due to partial self-sinking behavior,

Characterization and reproducibility

All experiments were done three times to make sure the results were accurate and consistent. The chemical interactions and floc characteristics formed during the coagulation process were investigated using zeta potential analysis (Otsuka), ATR-FTIR spectroscopy (PerkinElmer), and scanning electron microscopy (SEM; Hitachi). Zeta potential, ATR-FTIR, and SEM analyses were performed using samples obtained under the optimal coagulation conditions identified in this study, in order to elucidate the dominant interaction mechanisms responsible for microplastic removal.

Zeta potential measurements were carried out at ambient temperature using aqueous supernatant samples collected after the coagulation and settling stages, representing the post-treatment surface charge conditions. ATR-FTIR spectra were recorded in the range of 4000–400 cm^{-1} with a resolution of 4 cm^{-1} to identify functional groups and interaction-related spectral changes. SEM observations were conducted to examine surface morphology and floc structure after coagulation. Prior to imaging, the samples were coated with gold (Au) to enhance conductivity. All samples were prepared following an identical protocol to minimize potential preparation-induced artifacts. Drying was performed at moderate temperatures (40–60 °C), which are insufficient to induce thermal degradation or chemical modification of polyethylene or polystyrene.

Artificial neural network (ANN)

The implementation of the ANN model for predicting microplastic removal efficiency was based on a total of 56 experimental data points obtained from systematic coagulation experiments involving PE and PS microplastics. The input variables consisted of pH, chitosan dosage, slow mixing time, $CaCl_2$ dosage, tannic acid dosage, and microplastic type (PE or PS), while the output variable was the percentage removal efficiency. The dataset was then processed using SPSS, where it was divided into two subsets: 67.9% of the data was allocated for model training and 32.1% for model testing. In SPSS, the ANN architecture was configured to include an input layer comprising six neurons, a single hidden layer with four neurons employing the hyperbolic tangent activation function, and an output layer using an identity activation function to predict continuous values. Model training was conducted using the Neural Networks module in SPSS, which iteratively optimized synaptic weights until the minimum training error was reached.

Upon completion of the training phase, the model was evaluated using the testing dataset to assess its generalization performance on unseen data. The training and testing outputs, including error values and synaptic weights, were analyzed to identify the underlying relationships among variables and detect potential overfitting, indicated by an increase in testing error. In cases where overfitting was observed, optimization could be pursued by adjusting network parameters in SPSS, applying regularization techniques (where available), or implementing cross-validation. Additionally, expanding the dataset and incorporating new relevant input features may further enhance predictive accuracy. Once optimized, the ANN model can serve as a predictive tool for estimating microplastic removal efficiency under varying experimental conditions, thereby supporting the development of more effective coagulation strategies for water treatment (Gyparakis et al., 2025).

Data analysis

Data are expressed as mean ± standard deviation (SD). A one-way analysis of variance (ANOVA) was conducted at a 95% confidence level (α =

0.05) to assess significant differences in microplastic removal efficiency among treatments. When significant differences were detected ($P < 0.05$), to specifically identify the differences between groups, a follow-up analysis was conducted using Duncan's multiple range test (DMRT). All statistical analyses were performed using IBM SPSS Statistics version 27.0 (IBM Corp., Armonk, NY, USA).

RESULTS AND DISCUSSION

Microplastic coagulation with chitosan

Effect of pH on coagulation efficiency

The system pH plays a crucial role in regulating the coagulation efficiency of chitosan for microplastic removal (Figure 1). A significant influence of pH on chitosan's coagulation performance was observed for both PE and PS microplastics (one-way ANOVA, $p < 0.05$).

Under acidic conditions (pH 5–6), the microplastic removal efficiency remained low (<10%) and showed no significant differences ($p > 0.05$). This low efficiency is attributed to the protonation of chitosan's amino groups ($-NH_2$), which exist predominantly in the protonated form $-NH_3^+$ under acidic conditions, thereby keeping chitosan in a fully soluble state (Dongre, 2022). However, as the pH increases toward neutral to slightly alkaline conditions (pH 7–9), the coagulation efficiency increases significantly. This improvement is caused by the deprotonation of chitosan at higher pH values, where the amino groups ($-NH_2$) become neutral again, rendering chitosan insoluble and allowing it to form a gel-like structure (Lamanna et al., 2023). This gelation process enhances the ability of chitosan to interact with microplastic particles, thereby improving adsorption and coagulation. At pH 7, PS achieved a removal efficiency of 29.97 ± 12.30%, whereas PE reached 11.50 ± 2.81%. The highest removal efficiency was recorded at pH 9, although it did not differ significantly from the efficiencies observed at pH 7 and 8 ($p > 0.05$).

These results are consistent with the findings of (He et al., 2024; Huang et al., 2023), who reported low removal efficiency under acidic conditions (pH 5–6) but a significant increase at neutral to slightly alkaline pH (7–9). Duncan's test revealed significant differences ($p < 0.05$) compared to acidic conditions, confirming the positive influence of near-neutral to alkaline pH on the performance of chitosan. Similar observations were reported by (Agarwal et al., 2024; Huang et al., 2023), who attributed this improvement to charge neutralization and polymer bridging mechanisms.

However, (Prasetyo et al., 2025) documented a different trend, in which the highest polyethylene microplastic removal (81.5%) occurred at pH 6.0 using 100 mg/L chitosan, while efficiency declined at higher pH values (≥8) due to colloidal restabilization when chitosan becomes negatively charged. This discrepancy is likely related

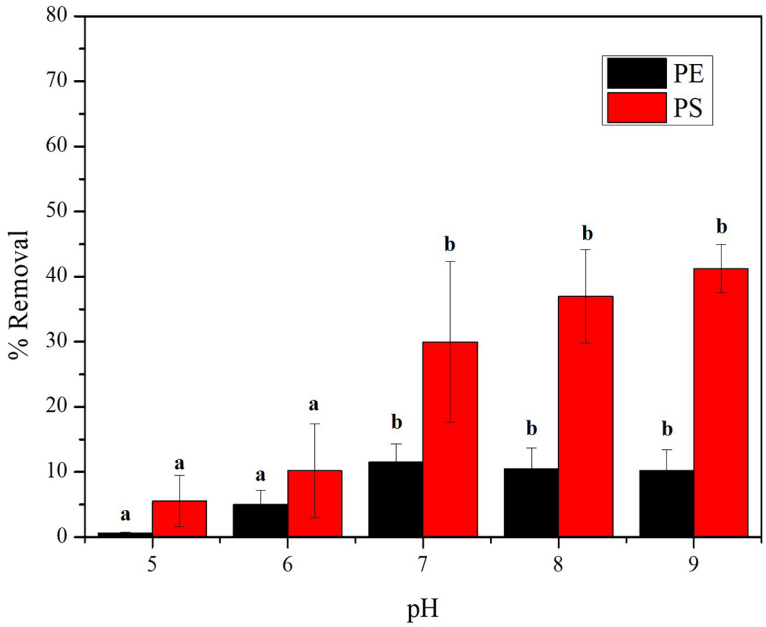

Figure 1. Effect of pH on coagulation using chitosan

to variations in microplastic particle size, which can substantially influence surface charge interactions and polymer bridging behavior.

Effect of chitosan dosage

Based on the experimental results, pH 7 was selected as the optimum condition for both types of microplastics, as it yielded the highest removal efficiency for PE and showed no significant difference compared to pH 8–9 for PS ($p > 0.05$). Therefore, pH 7 was used as the fixed condition for subsequent experiments involving variations in coagulant dosage. At the optimum pH of 7, chitosan dosages ranging from 0 to 300 mg/L were tested to evaluate their influence on microplastic removal (Figure 2). Statistical analysis using one-way ANOVA followed by Duncan's test ($p < 0.05$) indicated that coagulant dosage had a significant effect on the removal efficiency of both PE and PS microplastics.

For PE (Figure 2a), the removal efficiency increased from 0.73 ± 0.56% in the absence of chitosan to 18.53 ± 6.24% at a dosage of 250 mg/L, with no significant differences ($p > 0.05$) observed between 150–250 mg/L. This indicates that 250 mg/L represents the optimum dosage. The improvement in efficiency is primarily attributed to the sweep flocculation mechanism, in which chitosan flocs effectively entrap microplastic particles. However, beyond this dosage, the efficiency decreased due to floc saturation and floc breakage during the mixing process (Prasetyo et al., 2025). Given its hydrophobic nature and poor dispersibility in water, PE lacks the ability to settle on its own (Guo et al., 2024). Therefore, the sedimentation of PE relies entirely on the addition of the coagulant, and its removal efficiency is calculated solely based on the amount of coagulant introduced, without subtracting the blank value.

In contrast, for PS (Figure 2b), a similar yet more pronounced pattern was observed. The removal efficiency increased significantly ($p < 0.05$) from 7.52 ± 0.74% to 47.66 ± 6.36% at a dosage of 200 mg/L. The higher removal efficiency of PS compared to PE with increasing chitosan dosage can be attributed to its higher density and stronger polymer bridging interactions with chitosan, as well as more robust aggregation following destabilization, which results in the formation of more compact and stable flocs as the coagulant dosage increases. Conversely, the lower-density PE particles exhibit weaker bridging and slower settling behavior, thus requiring higher chitosan dosages to achieve comparable removal efficiencies (Avazpour and Noshadi, 2024). However, at dosages exceeding 200 mg/L, excess chitosan leads to charge reversal and restabilization of particles, thereby reducing the removal efficiency (Li et al., 2021). PS is more readily dispersible in water and possesses the ability to settle naturally without the addition of a coagulant, resulting in a more inherent sedimentation process. Therefore, for PS, the removal efficiency was calculated by subtracting the blank removal value (15.86 ± 1.86%) to ensure that the observed sedimentation of PS was attributable to the added coagulant rather than its inherent self-sinking capability.

Effect of slow mixing time

The effect of slow mixing time on the coagulation efficiency of PE and PS microplastics using chitosan is shown in Figure 3. Slow mixing plays an essential role in enhancing particle–particle collisions and facilitating the aggregation of microplastics into stable flocs during the

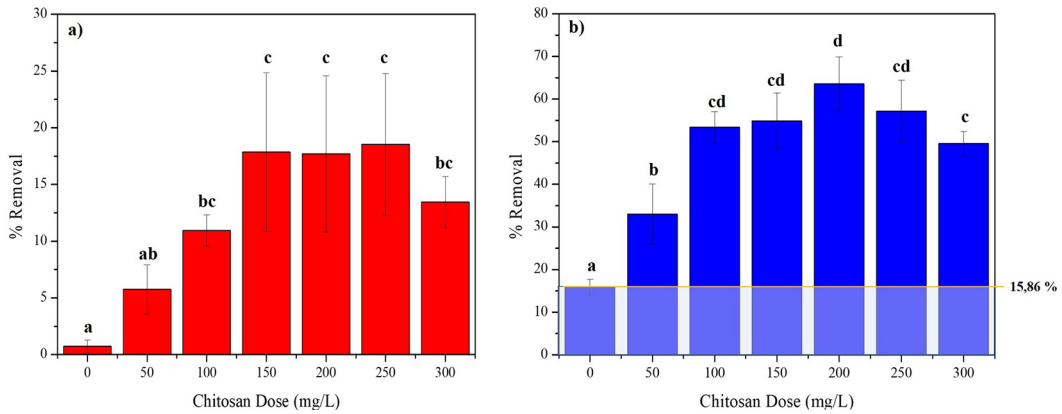

Figure 2. Effect of dosage on coagulation with chitosan: (a) polyethylene, (b) polystyrene

coagulation–flocculation process (Zhang et al., 2013). For PE (Figure 3a), the highest removal efficiency (22.96 ± 4.72%) was achieved without slow mixing (0 min), and it decreased significantly with increasing mixing time ($p < 0.05$). This indicates that the flocs formed are weak and easily disrupted by shear forces, consistent with the hydrophobic nature of PE, which limits electrostatic interactions and hydrogen bonding with chitosan (Arvaniti et al., 2021; Zhou et al., 2021). Consequently, sweep flocculation is the dominant mechanism, and prolonged mixing likely leads to floc fragmentation and the redispersion of particles. In contrast to previous studies reporting improved coagulation efficiency with prolonged slow mixing (Zhang et al., 2013), our results indicate that extended mixing is detrimental for polyethylene microplastics, which is attributed to the formation of weak, shear-sensitive flocs that are prone to breakage under shear.

In contrast, PS microplastics (Figure 3b) exhibited a different behavior, where the removal efficiency increased from 32.78 ± 0.78% (0 min) to 50.27 ± 1.02% at 10 minutes and then remained relatively stable up to 25 minutes. Statistical analysis showed that the efficiencies at 10–20 minutes were significantly higher than at 0 minutes ($p < 0.05$), confirming the importance of sufficient mixing duration for optimal floc growth. The aromatic structure of PS enables these additional interactions, resulting in higher removal performance compared to PE (Huang et al., 2023; Zhou et al., 2021). In addition, the stabilization of efficiency after 10 minutes is consistent with coagulation theory reported for PACI, where slow mixing must be sufficiently long to allow collisions and aggregate formation; however, once the flocs reach a stable size, further mixing does not significantly improve efficiency and may even cause fragmentation due to shear forces if prolonged excessively (Zhang et al., 2013). Thus, the plateau observed in this study indicates that PS flocs had achieved optimal structural stability after 10 minutes of slow mixing, resulting in no further improvement at longer durations.

Overall, these findings demonstrate that optimizing the slow mixing time is crucial for maximizing the coagulation performance of chitosan. The higher efficiency observed for PS compared to PE reinforces the importance of surface chemistry and polymer–particle affinity in governing microplastic removal behavior (Agarwal et al., 2024; Huang et al., 2023; Raj et al., 2024). This decrease can be attributed to floc breakage caused by excessive shear forces during the slow mixing phase, resulting in smaller flocs that subsequently resuspend in the water column (Li et al., 2024).

Effect of tannic acid and $CaCl_2$ addition

Effect of $CaCl_2$ dosage on microplastic removal

The removal efficiency of PS was consistently higher than that of PE under the same conditions. This is primarily attributed to the more negative surface charge of PS (Figure 6b), which enhances electrostatic attraction toward the protonated amine groups of chitosan and strengthens its interactions with Ca^{2+} ions. Calcium ions act as cation bridges that link negatively charged sites on microplastics with chitosan, while simultaneously

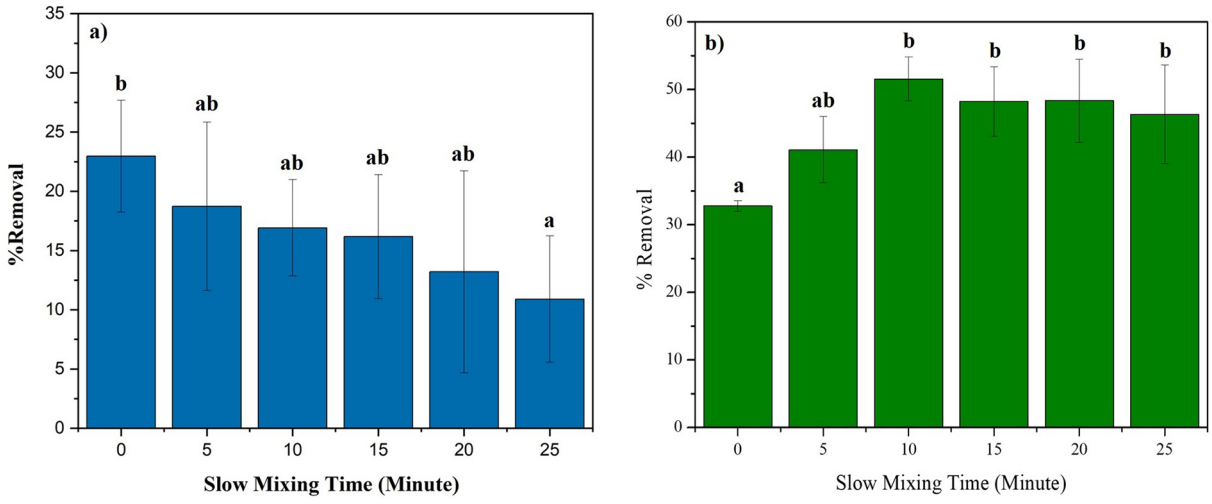

Figure 3. Effect of slow mixing time on coagulation using chitosan: (a) polyethylene (PE), (b) polystyrene (PS)

compacting the floc structure by reducing the thickness of the electrical double layer (Atmani et al., 2021). In contrast, the highly hydrophobic and nonpolar nature of PE limits ionic bridging and polymer adsorption, resulting in weaker interactions with the chitosan-Ca^{2+} system and consequently lower removal efficiency. Figure 4 illustrates the effect of varying $CaCl_2$ dosages on the removal efficiency of PE and PS microplastics using chitosan as the primary coagulant. In general, the addition of $CaCl_2$ tends to enhance coagulation efficiency up to a certain dosage, after which the effect stabilizes or decreases at higher concentrations.

For PE microplastics (Figure 4a), the removal efficiency increased slightly from 22.96 ± 4.72% in the absence of $CaCl_2$ to 25.39 ± 2.72% at a dosage of 500 mg/L, with no statistically significant differences (as indicated by the identical letter "a" in the graph). This suggests that the presence of Ca^{2+} has a limited influence on the chitosan-PE system. The highly hydrophobic nature of PE results in minimal contribution of Ca^{2+} to charge neutralization. Instead, Ca^{2+} primarily contributes by reducing the thickness of the electrical double layer and enhancing physical bridging (polymer bridging) between chitosan and the microplastics. Thus, the main role of $CaCl_2$ in this system is electrolyte screening compressing the electrical double layer and reducing interfacial electrostatic repulsion rather than direct electrostatic coagulation.

In contrast, for PS microplastics (Figure 4b), the effect of $CaCl_2$ was much more pronounced. The removal efficiency increased from 50.27 ± 1.02% in the absence of $CaCl_2$ to a maximum of 54.38 ± 1.55% at a dosage of 250 mg/L, before decreasing again at 500 mg/L. This increase indicates that Ca^{2+} ions play an important role in strengthening ionic interactions between functional groups on the PS surface and the positively charged amine groups of chitosan, thereby forming more stable ionic bridges (Chen et al., 2020). However, at excessively high dosages, surplus Ca^{2+} ions may cause over-neutralization of the negative charges on particle surfaces, reducing interparticle attraction and leading to colloidal restabilization (Chen et al., 2020; Zhou et al., 2021).

This mechanism is consistent with studies employing Moringa seed extract supplemented with $CaCl_2$ (Avazpour and Noshadi, 2024), in which the presence of Ca^{2+} was shown to compress the diffuse layer of the electric double layer surrounding particles in water. Compression of this double layer reduces electrostatic repulsion between particles, thereby strengthening aggregation and enhancing microplastic coagulation efficiency (Carvalho et al., 2016). Under these conditions, Ca^{2+} ions derived from $CaCl_2$ play a critical role in maintaining coagulation performance. Divalent calcium ions are more effective than monovalent cations in compressing the electrical double layer of microplastics, thus reducing interparticle repulsion. In addition, Ca^{2+} acts as a bridging ion that forms coordination interactions between deprotonated groups on chitosan and negatively charged sites on the microplastic surface (Baykara et al., 2024), with the predicted mechanism illustrated in Figure 11.

Effect of tannic acid dosage on microplastic removal

The variation in tannic acid dosage showed a clear influence on the performance of chitosan in removing PE and PS microplastics, as shown

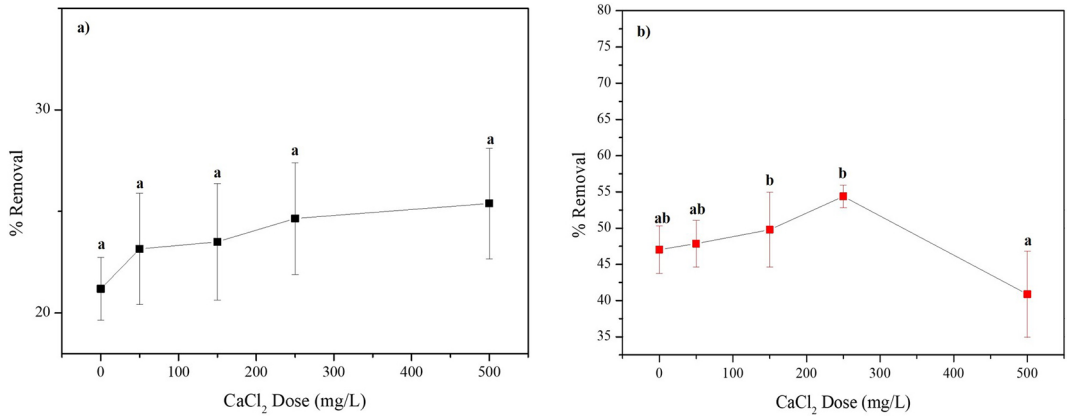

Figure 4. Effect of $CaCl_2$ addition on chitosan coagulation: (a) polyethylene (PE), (b) polystyrene (PS)

in Figure 5. Overall, the addition of tannic acid produced different effects on the two types of microplastics.

For PE microplastics (Figure 5a), the removal efficiency decreased sharply with increasing tannic acid dosage. In the absence of tannic acid (0 mg/L), chitosan was able to remove 22.96 ± 4.72% of the microplastics; however, this value declined upon the addition of tannic acid. This reduction indicates that tannic acid can strongly interact with the positively charged amino groups of chitosan through hydrogen bonding and electrostatic interactions (An et al., 2019), thereby hindering the ability of chitosan to bind to the highly hydrophobic PE surface. As a result, floc formation becomes less effective.

In contrast, for PS microplastics (Figure 5b), the removal efficiency increased significantly, reaching 61.58 ± 0.99% at a tannic acid dosage of 50 mg/L, before gradually decreasing at higher concentrations. This initial increase is attributed to the formation of a stable chitosan–tannic acid complex with dual binding capability toward PS particles through π–π interactions between the aromatic rings of tannic acid and the phenyl groups of polystyrene (An et al., 2019; J. Li, 2022). However, at excessive tannic acid dosages (>200 mg/L), the efficiency declined again, likely because the surplus tannic acid forms a protective layer (shielding effect) around the microplastic particles or chitosan, thereby inhibiting polymer bridging and effective floc formation.

The mechanism of coagulation

The analysis of zeta potential, FTIR spectra, and SEM provides a comprehensive understanding of the mechanisms governing microplastic removal in the chitosan-based system. As illustrated in Figure 11, the combined results from SEM, FTIR, and zeta potential confirm that chitosan interacts with microplastic surfaces through multiple pathways, including hydrogen bonding and coordination with Ca^{2+} ions or the phenolic groups of tannic acid. The addition of Ca^{2+} enhances charge neutralization and promotes the formation of ionic bridging between chitosan chains, whereas tannic acid strengthens adsorption through hydrogen bonding and π–π interactions. Collectively, these synergistic effects lead to improved floc formation, reduced surface charge, and enhanced stability of the aggregated microplastic flocs.

Zeta potential analysis

Zeta potential values serve as a key indicator of colloidal stability and the dominant coagulation–flocculation mechanisms. Systems with high zeta potential values (greater than ±30 mV) exhibit stable particles due to strong electrostatic repulsion, whereas values approaching zero indicate charge neutralization, enabling particles to aggregate into flocs and settle (Khoshnevisan and Barkhi, 2015; Malvern Ltd., 2011). The zeta potential analysis results are presented in Figure 6.

In this study, the initial zeta potential of PE was −15.58 mV, whereas PS exhibited a much

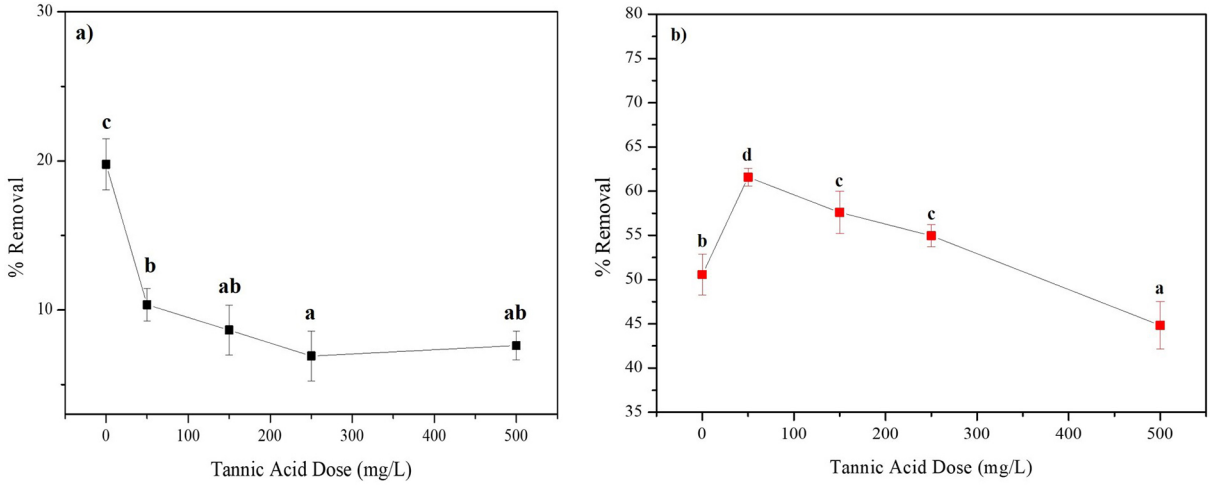

Figure 5. Effect of tannic acid dosage on chitosan-assisted coagulation: (a) polyethylene (PE), (b) polystyrene (PS)

more negative value of −64.53 mV, confirming that PS possesses higher dispersion stability due to its greater surface charge. After the addition of chitosan, the zeta potential increased to −4.45 mV for PE and −8.97 mV for PS, indicating that the positively charged amino groups of chitosan were adsorbed onto the microplastic surfaces, thereby reducing their negative charge. The zeta potential of PS increased from −64.5 to −8.9 mV following chitosan addition, signifying charge neutralization through the adsorption of $–NH_3^+$ groups. Further addition of Ca^{2+} shifted the value to −3.3 mV, suggesting the formation of ionic bridging and compression of the electrical double layer. Zeta potential values approaching zero are consistent with the formation of dense flocs observed visually, confirming that aggregation was dominated by charge neutralization mechanisms. Continued addition of $CaCl_2$ further reduced the zeta potential to −1.07 mV (PE) and −3.27 mV (PS), indicating the formation of Ca^{2+}-mediated ionic bridges between chitosan and the microplastic particles (Z. Chen et al., 2020).

In the chitosan–tannic acid system, the zeta potential increased slightly compared to the $CaCl_2$ system (−5.12 mV for PE and −2.54 mV for PS), indicating that charge neutralization still occurred; however, the dominant removal mechanism shifted toward polymer adsorption and hydrogen bonding mediated by the aromatic hydroxyl groups of tannic acid. Interestingly, the removal efficiency of PE decreased after the addition of tannic acid, even though the zeta potential approached zero. This may be attributed to weaker specific surface interactions with PE, which is highly hydrophobic and lacks sufficient active functional groups, causing tannic acid to provide no enhancement in sedimentation and potentially interfering with chitosan adsorption on its surface. Conversely, the removal efficiency of PS increased in the presence of tannic acid. The aromatic rings of PS can interact with the phenolic groups of tannic acid through π–π stacking (Li et al., 2022) and form hydrogen bonds with polar groups on both chitosan and tannic acid (An et al., 2019). These specific interactions enhance the surface affinity of PS toward the coagulant system, facilitating the formation of more stable aggregates and resulting in more effective coagulation compared to PE. Therefore, although the final zeta potentials of both microplastics approached zero, the differences in surface properties explain the observed disparity in removal efficiencies between PE and PS. These findings are consistent with DLVO theory, which accounts for the contribution of specific chemical forces such as hydrogen bonding, π–π interactions, and ionic bridging in addition to electrostatic and van der Waals forces (Derjaguin, 1987; Rahman et al., 2024).

FTIR analysis

The FTIR spectra of the pristine PE and PS microplastics exhibit characteristic absorption features corresponding to their polymer structures. For PE (Figure 7), the intense bands at 2916 and 2848 cm^{-1} are associated with the asymmetric and symmetric stretching vibrations of $-CH_2$ groups, while the peaks at 1470 and 720 cm^{-1} are attributed to CH_2 bending and rocking modes, respectively, confirming the saturated aliphatic nature of PE (Amelia et al., 2016; Veerasingam et al., 2020). PS (Figure 7) shows distinct aromatic peaks at 3025

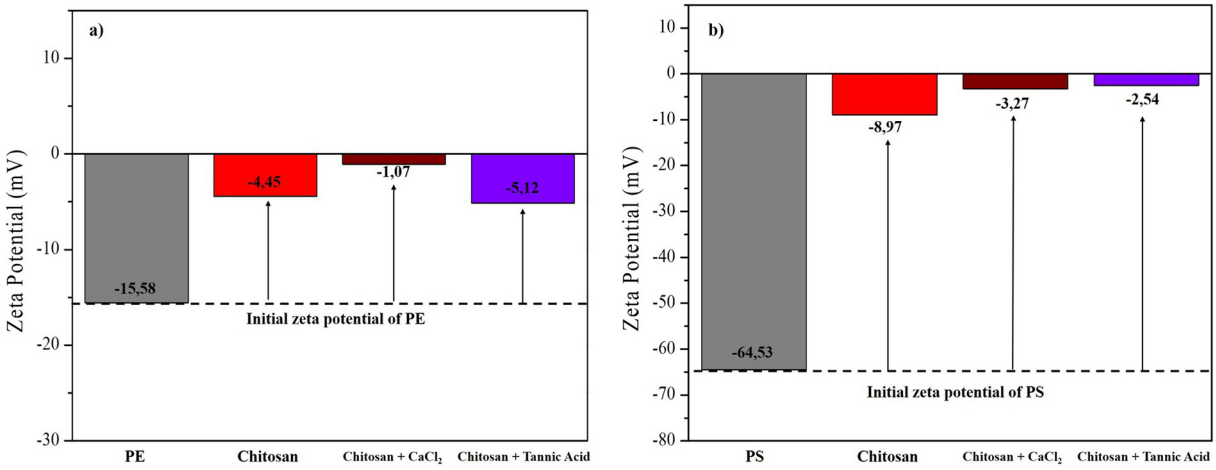

Figure 6. Zeta potential of: (a) Polyethylene (PE), (b) Polystyrene (PS)

cm^{-1} (C–H stretching), 1600 and 1490 cm^{-1} (C=C stretching of the benzene ring), and 700 cm^{-1} (out-of-plane C–H bending) (Veerasingam et al., 2020).

After coagulation with chitosan, both PE and PS microplastics retained their characteristic hydrocarbon bands at 2915 and 2848 cm^{-1} (C–H stretching) as well as 1470 and 720 cm^{-1} (CH_2 bending), although with noticeably reduced intensities. This attenuation indicates the formation of an organic layer on the microplastic surfaces due to adsorption and partial encapsulation by chitosan. Following the addition of $CaCl_2$, slight shifts were observed in the broad O–H/N–H stretching band (~3400 cm^{-1}) and the amide I band (~1650 cm^{-1}), suggesting coordination between Ca^{2+} ions and the hydroxyl and amino groups of chitosan. Such coordination promotes the formation of ionic bridges between chitosan chains and compresses the electrical double layer surrounding the negatively charged microplastics, consistent with the zeta potential values shifting toward neutrality (Figure 8).

These findings confirm that charge neutralization and ionic coordination synergistically enhance floc formation and aggregation stability. In the chitosan–tannic acid system, more pronounced spectral changes were detected, including red shifts in the O–H/N–H stretching bands and reductions in the intensities of the C=O and C–O peaks. These changes reflect strong hydrogen bonding and π–π stacking interactions between tannic acid, chitosan, and the aromatic rings of PS. Specifically for PS, the O–H/N–H stretching band shifted from 3405 cm^{-1} to 3388 cm^{-1}, and the amide I band from 1652 cm^{-1} to 1646 cm^{-1}, indicating the presence of hydrogen bonding and coordination with Ca^{2+} ions. The concurrent shift of zeta potential values toward less negative regions further confirms that these intermolecular interactions collectively promote aggregation. In contrast, PE exhibited only minor spectral shifts, indicating weaker surface adsorption and less pronounced charge compensation, consistent with its lower surface polarity.

SEM analysis

SEM analysis was conducted to examine the surface morphology and aggregation behavior of the flocs formed under different coagulation conditions. The SEM micrographs for each treatment are presented in Figures 9–10.

As shown in Figure 9a, the pristine PE particles exhibit a relatively smooth and compact surface with an irregular, flake-like structure (Wen et al., 2021), indicating the absence of surface modification. After the addition of chitosan (Figure 9b), the PE surface becomes rougher, and several aggregated domains appear, suggesting that chitosan molecules adhere to the microplastic

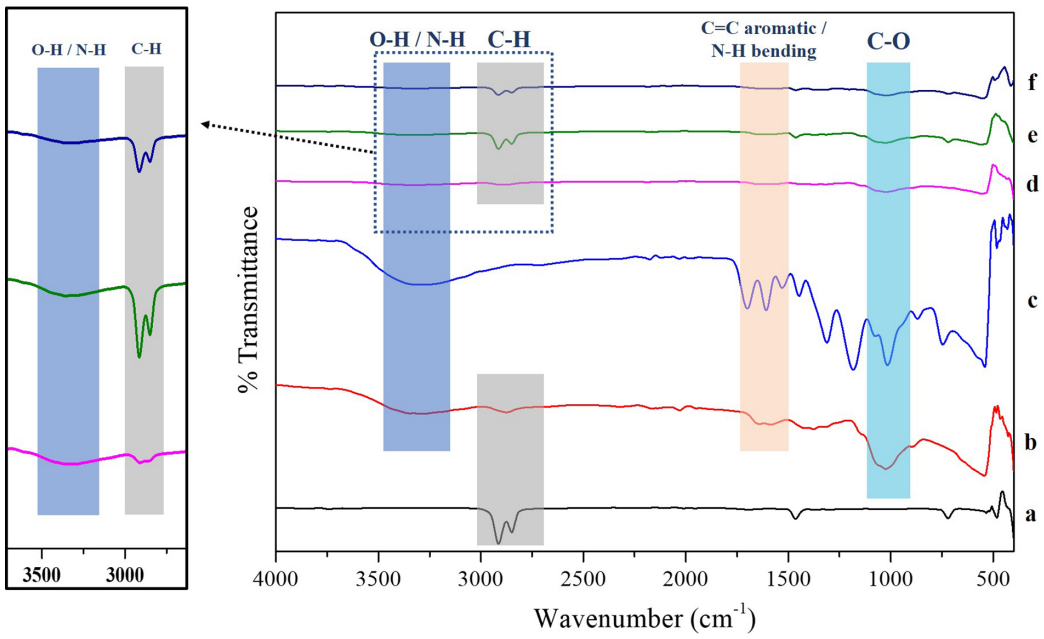

Figure 7. FTIR spectra of (a) microplastic PE, (b) chitosan, (c) tannic acid, (d) MPs after coagulation with chitosan, (d) MPs after coagulation with chitosan + $CaCl_2$, (e) (d) MPs after coagulation with chitosan + tannic acid

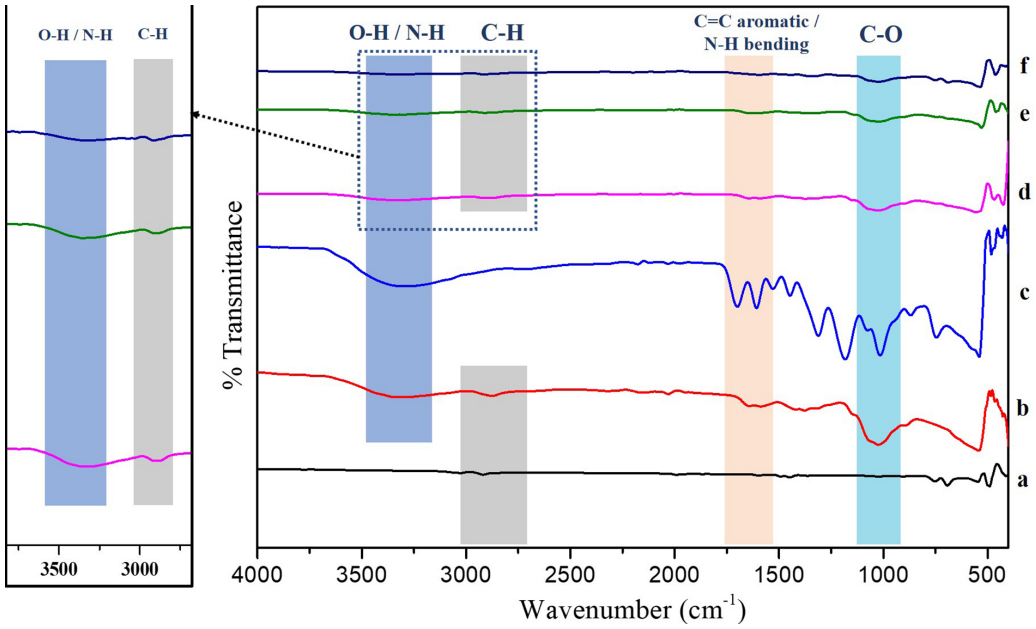

Figure 8. FTIR spectra of (a) microplastic PS, (b) chitosan, (c) tannic acid, (d) MPs after coagulation with chitosan, (d) MPs after coagulation with chitosan + $CaCl_2$, (e) (d) MPs after coagulation with chitosan + tannic acid

surface through electrostatic attraction and hydrogen bonding. A more compact and denser surface morphology is observed in the PE-chitosan-$CaCl_2$ composite (Figure 9c).

The presence of calcium ions promotes the formation of ionic bridges between the amine groups of chitosan and the negatively charged sites on the PE surface, thereby enhancing floc formation and surface coverage. This indicates that Ca^{2+} acts as a bridging agent that strengthens particle–polymer interactions, resulting in larger and denser flocs. In contrast, the PE-chitosan-tannic acid composite (Figure 9d) exhibits a more irregular and porous structure compared to the $CaCl_2$ system. This morphology is likely attributed to hydrogen bonding between tannic acid and chitosan (Atmani et al., 2021), which produces a more open network structure rather than compact aggregates. The presence of voids in this sample suggests that tannic acid promotes interparticle connections but with less uniform surface coverage than that achieved through $CaCl_2$ crosslinking. This observation corresponds to the lower PE removal efficiency obtained when tannic acid was added.

The untreated PS particles (Figure 10a) exhibit angular shapes with relatively smooth surfaces and remain individually dispersed. After coagulation with chitosan (Figure 10b), the PS particles appear to be partially adsorbed and display a rougher surface with several regions covered by a thin layer. These changes indicate the adsorption of chitosan through weak electrostatic interactions and hydrogen bonding, which subsequently facilitates polymer bridging and initiates the aggregation process.

In the chitosan-$CaCl_2$ system (Figure 10c), the morphology of the PS residues exhibits a denser structure with more pronounced interparticle agglomeration. The presence of tightly connected domains indicates the formation of ionic crosslinking networks between Ca^{2+} and the amino and hydroxyl groups of chitosan. This cation-bridging mechanism produces flocs that are more compact and stable than those formed with chitosan alone.

Coagulation using chitosan-tannic acid (Figure 10d) results in a more layered and irregular morphology, with the particle surfaces being more extensively covered. This indicates the formation of chitosan-tannin complexes through hydrogen bonding (Atmani et al., 2021) and π–π interactions with the PS surface (Li, 2022), both of which contribute to increased floc density and stronger interparticle interactions.

Among the proposed coagulation mechanisms, charge neutralization is directly supported by zeta potential measurements. In contrast, ionic bridging by Ca^{2+} ions, hydrogen bonding, and possible π–π interactions are

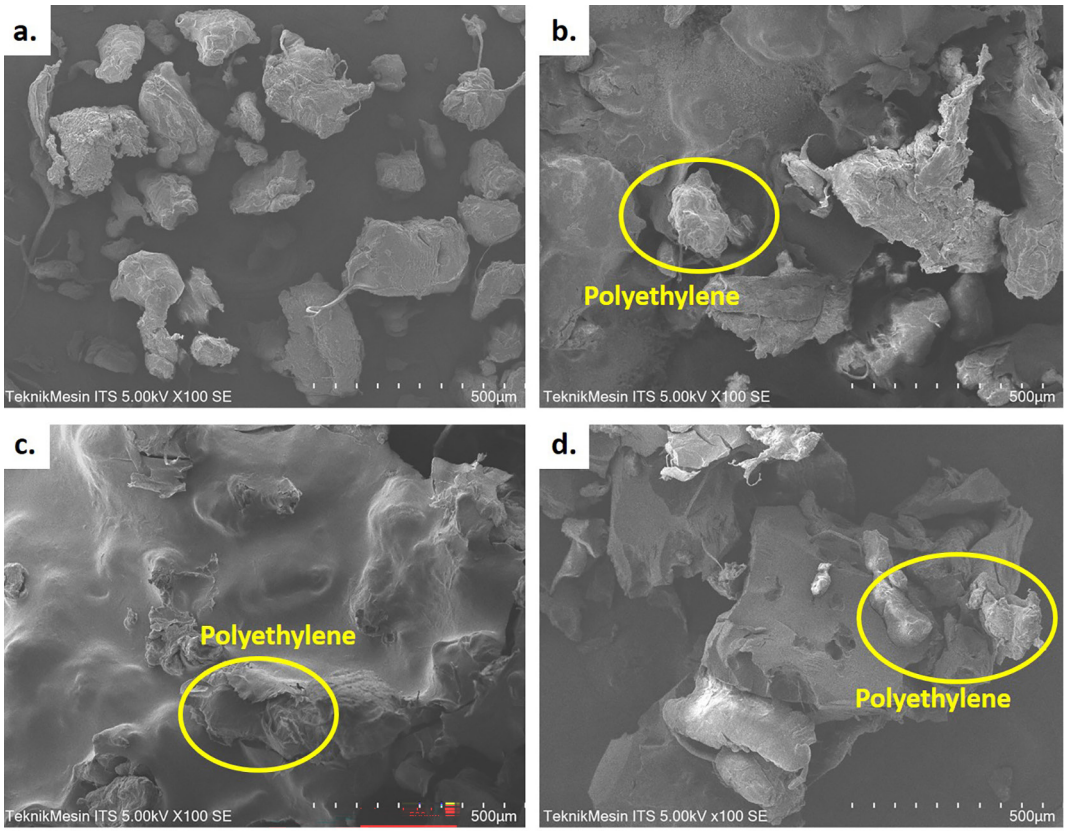

Figure 9. SEM micrographs of (a) PS before coagulation, (b) PS after coagulation with chitosan, (c) PS after coagulation with chitosan-$CaCl_2$, (d) PS after coagulation with chitosan-tannic acid

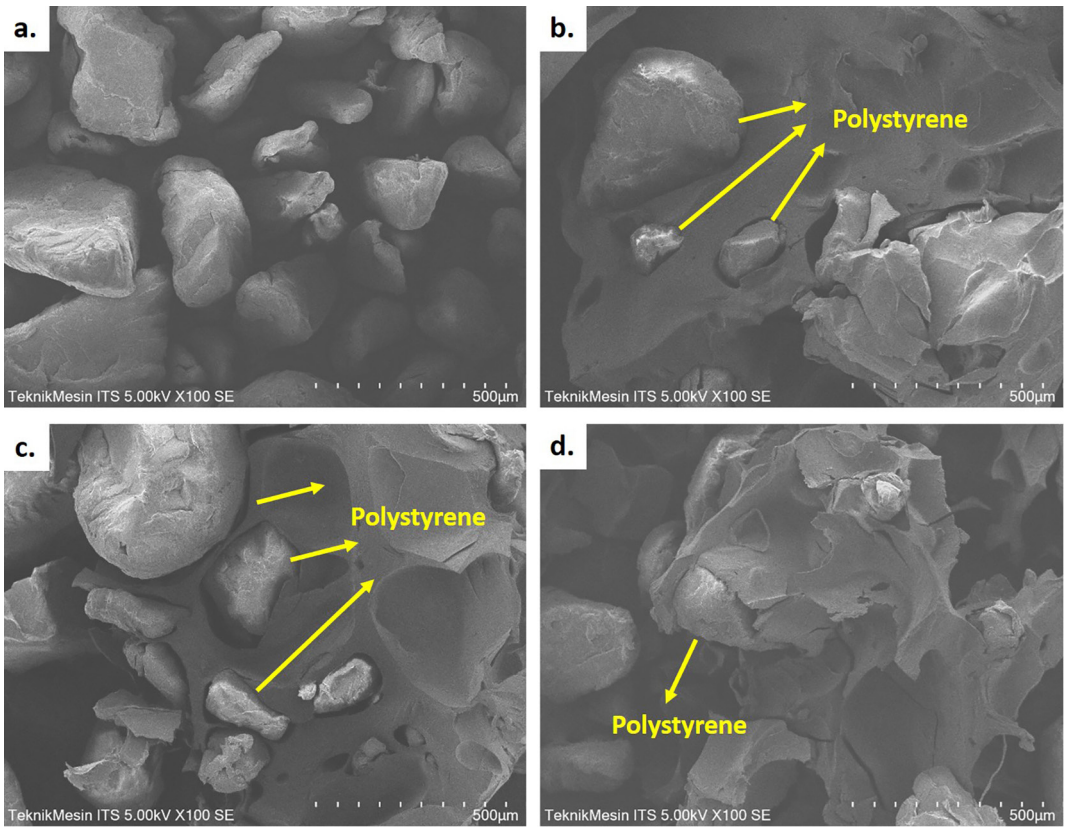

Figure 10. SEM micrographs of (a) PS before coagulation, (b) PS after coagulation with chitosan, (c) PS after coagulation with chitosan-$CaCl_2$, (d) PS after coagulation with chitosan-tannic acid

indirectly inferred based on FTIR spectral features, SEM observations, and consistency with previously reported studies, rather than being directly demonstrated.

The correlation among zeta potential, FTIR, and SEM analyses reveals the coagulation mechanisms operating in the chitosan, chitosan–$CaCl_2$, and chitosan–tannic acid systems. Together, these analyses illustrate the roles of charge neutralization, polymer and ionic bridging, as well as hydrogen bonding and π–π interactions in driving microplastic aggregation. The integration of these findings confirms that microplastic removal is governed by a combination of electrostatic mechanisms and specific chemical interactions, rather than solely by changes in surface charge.

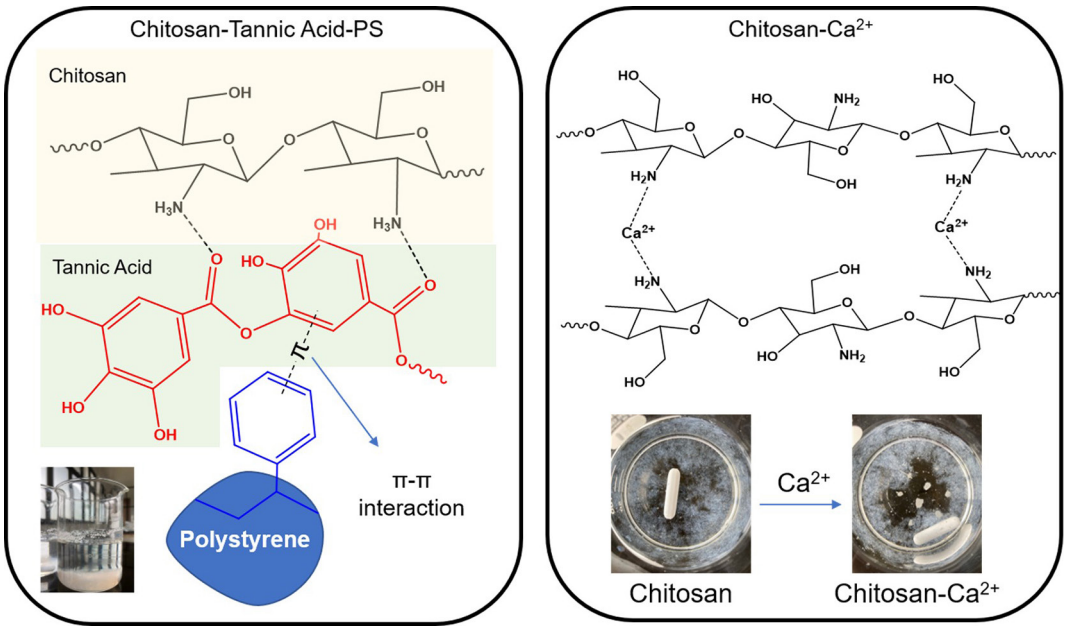

Figure 11. Proposed interaction mechanisms of chitosan-tannic acid and chitosan-Ca^{2+} in polystyrene microplastic coagulation

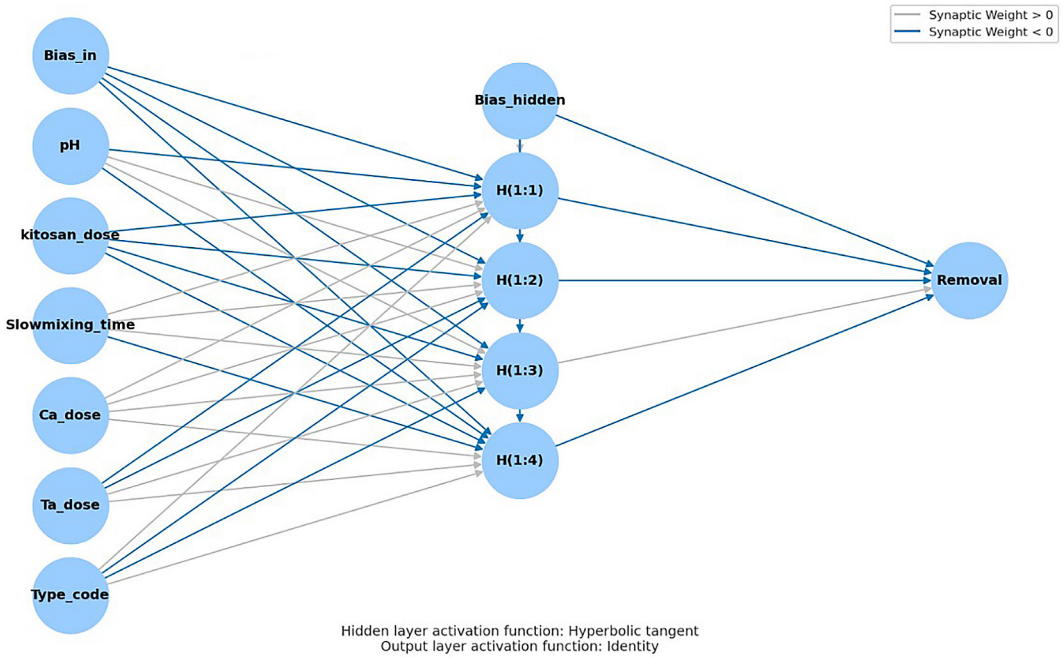

Figure 12. ANN modelling for MPs removal

ANN modeling analysis

The ANN model was divided into 67.9% for training and 32.1% for testing to balance the learning and evaluation processes. The input variables included pH, chitosan dosage, slow mixing time, $CaCl_2$ dosage, tannic acid dosage, and microplastic type (PE or PS). The network consisted of an input layer with six neurons, a single hidden layer with four neurons using a hyperbolic tangent activation function to capture nonlinear relationships, and an output layer with an identity activation function to predict removal efficiency as a continuous variable. Figure 12 illustrates the synaptic weights representing the influence of each input on the output. Positive weights (gray) indicate direct relationships, whereas negative weights (blue) indicate inverse correlations. These findings demonstrate how the model internalizes the complex interactions among system parameters that influence coagulation performance, such as pH and coagulant dosage.

The model evaluation showed strong learning performance during the training phase, with a sum of squares error (SSE) of 0.524 and a relative error of 0.028, indicating a good fit to the training data. However, the testing results showed an increase in SSE to 2.121 and relative error to 0.088, reflecting reduced accuracy and indicating the presence of overfitting. This suggests that although the model effectively memorized patterns in the training dataset, its ability to generalize to new data remains limited. To address this issue, model refinement is required through techniques such as adjusting the network architecture, applying regularization, and expanding the dataset. Incorporating additional relevant features such as environmental variables or more detailed microplastic characteristics may further enhance the model's predictive capability.

Overall, despite its limitations, the ANN model demonstrates potential for modeling the coagulation process for microplastic removal using chitosan. With further optimization and dataset expansion, this model could serve as a valuable predictive tool to support the development of efficient water treatment strategies for microplastic contamination.

CONCLUSIONS

This study demonstrates that chitosan-based systems enhanced with Ca^{2+} or tannic acid offer effective, fully metal-free alternatives for PE and PS microplastic removal. Optimal efficiency was achieved at near-neutral pH, where charge neutralization, ionic bridging, hydrogen bonding, hydrophobic interactions, and π–π stacking collectively promoted stable floc formation. Zeta potential, ATR-FTIR, and SEM analyses confirmed the formation of compact aggregates through synergistic electrostatic and chemical interactions, while the ANN model successfully captured the nonlinear behavior governing coagulation performance and was useful for trend analysis and system optimization within the studied conditions. From an application standpoint, the proposed system exhibits promising technical feasibility. Chitosan, $CaCl_2$, and tannic acid are readily available, low-cost materials suitable for scalable integration into existing water treatment infrastructures without major process modification. Their biodegradability and absence of toxic metals result in environmentally safer sludge compared to conventional Fe/Al coagulants, supporting compliance with emerging green-technology standards. Furthermore, the relatively low dosage requirements improve operational cost efficiency. To enable real-world deployment, future work should assess performance under variable water matrices, long-term floc stability, and potential reuse or valorization pathways for the produced biopolymer-based sludge.

Acknowledgements

The authors gratefully acknowledge the financial support provided by Universitas Andalas through the Program Magister menuju Doktor Sarjana Unggul (PMDSU) Batch I. This research was conducted under the research contract No. 116/UN16.19/PT.01.03/PMDSU/2025 for the Fiscal Year 2025.

REFERENCES

1. Agarwal, P., Prakash, S., Saini, G. (2024). Natural coagulants (*Moringa oleifera* and *Benincasa hispida*) based removal of microplastics. *Cleaner Water*, *1*, 100010.
2. Amelia, R. P. D., Gentile, S., Nirode, W. F., Huang,

L. (2016). Quantitative analysis of copolymers and blends of polyvinyl acetate (PVAc) using fourier transform infrared spectroscopy (FTIR) and elemental analysis (EA). *World Journal of Chemical Education*, *4*. https://doi.org/10.12691/wjce-4-2-1

3. An, X., Kang, Y., Li, G. (2019). The interaction between chitosan and tannic acid calculated based on the density functional theory. *Chemical Physics*, *520*(December 2018), 100–107. https://doi.org/10.1016/j.chemphys.2018.12.009
4. Arvaniti, O. S., Antonopoulou, G., Tsagkogianni, D., Stasinakis, A. S. (2021). Screening on the sorption of emerging contaminants to polystyrene and polyethylene and use of coagulation – flocculation process for microplastics' removal. *Global Nest Journal*, *23*(2), 303–308. https://doi.org/10.30955/gnj.003854
5. Atmani, H., Aboulouard, A., Bakkardouch, F. E., Laallam, L., Jouaiti, A., El idrissi, M. (2021). Physical and chemical aspects of the interaction of chitosan and cellulose acetate with ions Ca2+ and K+ using DFT methods. *Journal of Molecular Modeling*, *27*(4), 1–12. https://doi.org/10.1007/s00894-021-04715-2
6. Avazpour, S., Noshadi, M. (2024). Enhancing the coagulation process for the removal of microplastics from water by anionic polyacrylamide and natural-based Moringa oleifera. *Chemosphere*, *358*(April), 142215. https://doi.org/10.1016/j.chemosphere.2024.142215
7. Baykara, H., Riofrio, A., Garcia-Troncoso, N., Cornejo, M., Tello-Ayala, K., Flores Rada, J., Caceres, J. (2024). Chitosan-cement composite mortars: exploring interactions, structural evolution, environmental footprint and mechanical performance. *ACS Omega*, *9*(23), 24978–24986. https://doi.org/10.1021/acsomega.4c02040
8. Carvalho, M. S., Alves, B. R. R., Silva, M. F., Bergamasco, R., Coral, L. A., Bassetti, F. J. (2016). $CaCl_2$ applied to the extraction of *Moringa oleifera* seeds and the use for *Microcystis aeruginosa* removal. *Chemical Engineering Journal*, *304*, 469–475. https://doi.org/10.1016/j.cej.2016.06.101
9. Chen, J., Cai, S., Wang, Y., Huang, H. (2024). Enhanced removal of polyethylene microplastics from water through polymeric ferric sulfate with laminarin. *Process Safety and Environmental Protection*, *183*(December 2023), 307–314. https://doi.org/10.1016/j.psep.2024.01.036
10. Chen, P., Wang, Y., He, S., Wang, P., Xu, Y., Zhang, L. (2020). Green synthesis of spherical calcium hydroxide nanoparticles in the presence of tannic acid. *Advances in Materials Science and Engineering*, *2020*. https://doi.org/10.1155/2020/9501897
11. Chen, Z., Liu, J., Chen, C., Huang, Z. (2020). Sedimentation of nanoplastics from water with Ca/Al dual flocculants: Characterization, interface reaction, effects of pH and ion ratios. *Chemosphere*, *252*, 126450. https://doi.org/10.1016/j.chemosphere.2020.126450
12. Derjaguin, V. (1987). *The Derjaguin-Landau-Verwey- Overbeek (Dlvo) Theory Stability Of Lyophobic Colloids*. *1986*, 293–294.
13. Dongre, R. S. (2022). *Marine Polysaccharides in Pharmaceutical Uses: Chitin, Chitosan, Alginate, Marine Polysaccharides in Pharmaceutical Uses* (Issue March). https://doi.org/10.1007/978-3-030-42215-8
14. Du, J., Zhou, Q., Li, H., Xu, S., Wang, C., Fu, L., Tang, J. (2021). Environmental distribution, transport and ecotoxicity of microplastics: A review. *Journal of Applied Toxicology*, *41*(1), 52–64. https://doi.org/10.1002/jat.4034
15. Eamrat, R., Rujakom, S., Pussayanavin, T., Taweesan, A., Witthayaphirom, C., Kamei, T. (2024). Optimizing biocoagulant aid from shrimp shells (*Litopenaeus vannamei*) for enhancing microplastics removal from aqueous solutions. *Environmental Technology and Innovation*, *33*, 103457.
16. Guo, M., Noori, R., Abolfathi, S. (2024). Microplastics in freshwater systems: Dynamic behaviour and transport processes. *Resources, Conservation and Recycling*, *205*(December 2023), 107578. https://doi.org/10.1016/j.resconrec.2024.107578
17. Gyparakis, S., Trichakis, I., Daras, T., Diamadopoulos, E. (2025). Artificial neural networks (ANNs) and multiple linear regression (MLR) analysis modelling for predicting chemical dosages of a water treatment plant (WTP) of drinking water. *Water 17*(2).
18. He, J., Wang, W., Ni, F., Tian, D., Yang, G., Lei, Y., Shen, F., Zou, J., Huang, M. (2024). A novel hydrophobic chitosan-polyaluminum chloride composite flocculant for effectively simultaneous removal of microplastic and antibiotics composite pollution. *Separation and Purification Technology*, *337*, 126420.
19. Hidalgo-Ruz, V., Gutow, L., Thompson, R. C., Thiel, M. (2012). Microplastics in the marine environment: A review of the methods used for identification and quantification. *Environmental Science and Technology*, *46*(6), 3060–3075. https://doi.org/10.1021/es2031505
20. Huang, L., He, W., Zhang, Y., Wang, X., Wu, K., Yang, Z., Zhang, J. (2023). Chitosan enhances poly aluminum chloride flocculation system removal of microplastics: Effective, stable, and pollution free. *Journal of Water Process Engineering*, *54*(2), 103929. https://doi.org/10.1016/j.jwpe.2023.103929
21. Izabela, K. (2020). Aluminium drinking water treatment residuals and their toxic impact on human health. *Molecules*, *25*(3), 13.

22. Khoshnevisan, K., Barkhi, M. (2015). Information about Zeta Potential. *Encyclopedia of Membranes*, *May*, 2063–2064. https://doi.org/10.13140/RG.2.1.4554.3844
23. Koelmans, A. A., Mohamed Nor, N. H., Hermsen, E., Kooi, M., Mintenig, S. M., De France, J. (2019). Microplastics in freshwaters and drinking water: Critical review and assessment of data quality. *Water Research*, *155*, 410–422. https://doi.org/10.1016/j.watres.2019.02.054
24. Lamanna, L., Giacoia, G., Friuli, M., Leone, G., Carlucci, N., Russo, F., Sannino, A., Demitri, C. (2023). Oil-Water Emulsion Flocculation through Chitosan Desolubilization Driven by pH Variation. *ACS Omega*, *8*(23), 20708–20713.
25. Li, C., Busquets, R., Campos, L. C. (2024). Enhancing microplastic removal from natural water using coagulant aids. *Chemosphere*, *364*(August), 143145. https://doi.org/10.1016/j.chemosphere.2024.143145
26. Li, C., Busquets, R., Moruzzi, R. B., Campos, L. C. (2021). Preliminary study on low-density polystyrene microplastics bead removal from drinking water by coagulation-flocculation and sedimentation. *Journal of Water Process Engineering*, *44*, 102346.
27. Li, J. (2022). Effect of coagulation on microfibers in laundry wastewater. *Environmental Research*, *212*. https://doi.org/10.1016/j.envres.2022.113401
28. Li, W., Chen, X., Li, M., Cai, Z., Gong, H., Yan, M. (2022). Microplastics as an aquatic pollutant affect gut microbiota within aquatic animals. *Journal of Hazardous Materials*, *423*(PB), 127094. https://doi.org/10.1016/j.jhazmat.2021.127094
29. Ma, B., Xue, W., Ding, Y., Hu, C., Liu, H., Qu, J. (2019). Removal characteristics of microplastics by Fe-based coagulants during drinking water treatment. *Journal of Environmental Sciences (China)*, *78*, 267–275. https://doi.org/10.1016/j.jes.2018.10.006
30. Malvern Ltd. (2011). Zeta potential: An Introduction in 30 minutes. *Zetasizer Nano Serles Technical Note. MRK654-01*, *2*, 1–6.
31. Monira, S., Bhuiyan, M. A., Haque, N., Pramanik, B. K. (2021). Assess the performance of chemical coagulation process for microplastics removal from stormwater. *Process Safety and Environmental Protection*, *155*, 11–16. https://doi.org/10.1016/j.psep.2021.09.002
32. Prasetyo, S., Santos, C. A., Sugih, A. K., Kristianto, H. (2025). Utilization of chitosan as a natural coagulant for polyethylene microplastic removal. *Sustainable Chemistry for the Environment*, *9*, 100225.
33. Rahman, A. M. N. A. A., Rusli, A., Abdullah, M. K., Shuib, R. K., Hamid, Z. A. A., Ku Ishak, K. M., Mohd Zaini Makhtar, M., Jaafar, M., Shafiq, M. D. (2024). A review of microplastic surface interactions in water and potential capturing methods. *Water Science and Engineering*, *17*(4), 361–370. https://doi.org/10.1016/j.wse.2023.11.008
34. Raj, S., Mahanty, B., Hait, S. (2024). Coagulative removal of polystyrene microplastics from aqueous matrices using FeCl3-chitosan system: Experimental and artificial neural network modeling. *Journal of Hazardous Materials*, *468*.
35. Sixto-Berrocal, A. M., Vázquez-Aldana, M., Miranda-Castro, S. P., Martínez-Trujillo, M. A., Cruz-Díaz, M. R. (2023). Chitin/chitosan extraction from shrimp shell waste by a completely biotechnological process. *International Journal of Biological Macromolecules*, *230*(January). https://doi.org/10.1016/j.ijbiomac.2023.123204
36. Sotero-Santos, R. B., Rocha, O., Povinelli, J. (2007). Toxicity of ferric chloride sludge to aquatic organisms. *Chemosphere*, *68*(4), 628–636. https://doi.org/10.1016/j.chemosphere.2007.02.049
37. Veerasingam, S., Ranjani, M., Venkatachalapathy, R., Bagaev, A. (2020). Contributions of Fourier transform infrared spectroscopy in microplastic pollution research : A review. *Critical Reviews In Environmental Science and Technology*. https://doi.org/10.1080/10643389.2020.1807450
38. Wen, D., Chen, Y., Tong, Y., Wang, H., Zhang, H., Luo, Y. (2021). Quantification of microplastics in soils using accelerated solvent extraction: Comparison with a visual sorting method. *Bulletin of Environmental Contamination and Toxicology*, *Zhang 2020*, 1–8. https://doi.org/10.1007/s00128-021-03200-z
39. Zhang, Y., Wang, X., Li, Y., Wang, H., Shi, Y., Li, Y., Zhang, Y. (2022). Improving nanoplastic removal by coagulation: Impact mechanism of particle size and water chemical conditions. *Journal of Hazardous Materials*, *425*(November 2021), 127962. https://doi.org/10.1016/j.jhazmat.2021.127962
40. Zhang, Z., Liu, D., Hu, D., Li, D., Ren, X., Cheng, Y., Luan, Z. (2013). Effects of slow-mixing on the coagulation performance of polyaluminum chloride (PACI). *Chinese Journal of Chemical Engineering*, *21*(3), 318–323. https://doi.org/10.1016/S1004-9541(13)60463-2
41. Zhou, G., Chen, G., Tang, P., Li, X., Ma, J., Liu, B. (2025). Revealing the removal behavior of five neglected microplastics in coagulation-ultrafiltration processes: Insights from experiments and predictive modeling. *Journal of Hazardous Materials*, *491*(March), 137857. https://doi.org/10.1016/j.jhazmat.2025.137857
42. Zhou, G., Wang, Q., Li, J., Li, Q., Xu, H., Ye, Q., Wang, Y., Shu, S., Zhang, J. (2021). Removal of polystyrene and polyethylene microplastics using PAC and $FeCl_3$ coagulation: Performance and mechanism. *Science of the Total Environment*, *752*(2), 141837.